Estimation of effect of voids on frequency response of mountain tunnel lining based on microtremor method

Yang GAO[1), 2)], Yujing JIANG[1), 3)*], Bo LI[1)]

[1)] Graduate School of Engineering, Nagasaki University, Nagasaki 852-8521, Japan

[2)] Research Center of Geotechnical and Structural Engineering, Shandong University, Jinan 250061, China

[3)] Key Laboratory of Mine Disaster Prevention and Control, Shandong University of Science and Technology, Qingdao 266510, China

[*] Corresponding author. Tel: +81-95-819-2612. Fax: +81-95-819-2627. Email address: jiang@nagasaki-u.ac.jp

ABSTRACT: Nowadays, aged tunnels keep continuously increasing all over the world, which require effective inspection methods to assess their health conditions. In this study, both in-situ acceleration wave measurements and numerical simulations were carried out to study the microtremor characteristics of mountain tunnel lining. Power Spectrum Density (PSD) of signals was calculated and peak frequencies were identified using the peak-picking method. Discontinuous contacts between rock masses and lining concrete were simplified as weak interfaces with low stiffness, which play the role of elastic supporting during dynamic calculation. Influences of voids, rock type and concrete type on their peak frequencies were evaluated. The results of the numerical analysis show that the normal stiffness of rock-concrete interface has strong correlation with the magnitude of peak frequency. The frequency response of tunnel lining is affected by the presence of voids located around tunnel

circumference behind lining. The first peak frequency is dependent on the void size and location. The larger the void size and location angle, the greater the decrease of the first peak frequency. The peak frequency also decreases as the strength of concrete decreases, and is not affected by the change of properties of unweathered rock masses. Additional frequency modes can be identified when voids are not located on the central axis of tunnel. The first peak frequency variation can be considered to be intimately linked with the stress state of the tunnel lining influenced by the existence of voids.

Keywords : Tunnel lining; Microtremor; Void; Power spectrum density; Peak frequency

1.Introduction

As a primary support of tunnel excavation, concrete lining serves a number of functions, such as supporting adjacent ground, and resisting ground erosion and degradation. Voids, usually existing between concrete linings and rock masses, are unfavorable to the supporting system and may invoke lining structure failures, such as water leakage, reinforcement corrosion and cracking. Voids may be produced during construction especially under severe geological conditions, and may be generated later along with the degradation of lining and surrounding rock mass. Assessment of the influences of these unpredictable voids behind concrete linings on tunnel construction and maintenance is an important issue.

At present, a number of void inspection methods in both destructive and non-destructive manners have been proposed and used in practices. Representative ones include core sampling, ground penetrating radar (GPR), ultrasonic method, and magnetic method, etc. (Daniels, 2004; Jiles, 1990; Poranski et al., 1996). Coring provides specific information inside of tunnel lining within limited inspection areas, but is slow and expensive. Non-destructive methods could help improve investigation periods in relatively large areas. However, highly-experienced operators are essential in these inspections, and considerable time and cost are required to estimate the overall structural integrity in the most previous techniques (Park and Choi, 2008).

The existence of the voids changes the stiffness of the total supporting system and has a great influence on the natural frequency of a structure. Meanwhile, the natural frequency can be acquired conveniently by dynamic tests (Vestroni and Capecchi, 2000; Lee, 2004), which provides a possible approach for effectively detecting the voids between the tunnel lining and the rock mass.

There are two methods available for measuring the vibration response of a structure, including the forced vibration test and the ambient vibration test. Unlike other structures, the mountain tunnels are subjected to rock-structure interaction between the lining and its surrounding rock mass. Hence, their dynamic behavior is controlled by the stiffness of tunnel lining, the surrounding rock mass and the concrete-rock interface which exists between the surrounding rock mass and the tunnel lining (Wiehle, 1964). The forced vibration test is not applicable for the damage detection of large-scale structures, where huge reaction mass shakers are necessary (Peeters et al.,

2001). With the development and application of high sensitivity accelerometer, low-cost ambient tests have drawn more attention for the structural damage identification. The ambient vibration measurement is a kind of output data-only dynamic test and a modal analysis procedure is carried out based on the output data. Thus far, the ambient test has been applied to various types of structures, such as bridges (Magalhas et al., 2009), buildings (Michel et al., 2008), historical structures (Júlio et al., 2008), and mechanical structures (Pierro et al., 2008). Microtremor, as a type of ambient vibration originating from the natural or artificial oscillations without specific sources, has attracted lots of attentions in the recent studies on the dynamic behavior of concrete structures (e.g. Tuladhar et al., 2004; Chatelain et al., 2000; Ikeda et al., 2010). However, few attentions have been focused on the microtremor measurements for the damage identification of mountain tunnel linings (Gao et al., 2012; Jiang et al., 2012).

In numerical simulations, the Finite Element Method (FEM) is commonly adopted to predict structure vibrations. The presence of discontinuities in numerical models, such as the interfaces between tunnel linings and surrounding rock masses, however, would undermine the calculation accuracy in some degree, especially when large deformations occur. With the capability of simulating large deformations and non-linear dynamic calculation of discontinuities, the Distinct Element Method (DEM) has received extensive applications in recent years (Jiang et al. 2009; Zhang et al.1997). Zhao et al. (2006; 2008) conducted seismic wave propagation across single or multiple rock fractures by using the code of UDEC. Those simulation results,

including the reflection and transmission coefficients and the influence of joint stiffness on wave propagation, showed good agreements with theoretical calculations.

In this study, in-situ microtremor measurements were carried out on the surface of a mountain tunnel lining. The peak frequencies of the lining were identified from the measured acceleration data of ambient vibrations. Numerical simulations were performed by using the DEM to investigate the vibration behavior of tunnel lining. The influences of the voids and their geometrical parameters, rock type and concrete type on frequency response of tunnel lining were studied. The relationship between the peak frequency and the stress state of the tunnel lining were also discussed based on the numerical results.

2. In-situmicrotremor measurements of a tunnel lining

The measurements were carried out on the Satomi tunnel located in Sasebo City, Nagasaki Prefecture, Japan. The Satomi tunnel was built in 1992 with a length of 529 m. The thickness of lining concrete was designed as 70 cm. Some defects such as cracks and voids were firstly detected on the lining concrete after it was commissioned for around twenty years, due to the deterioration of lining concrete. According to the tunnel inspection results, two typical spans with different health conditions were chosen for microtremor measurements (marked as S1 and S2 as shown in Fig. 1).

Fig.1 Inspection results of spans S1 & S2. (a) S1: healthy span. (b) S2: damaged span,

where voids, three transverse cracks and one axial crack exist.

The measurement system consists of a power unit, a PC & data acquisition device and two accelerometers, as shown in Fig. 2. The traffic was regulated to one-way during measurements, therefore only two monitoring points on the crown and arch (C1 & C2, see Fig. 3) where voids often occur were selected to verify the inspection results during the limited measuring time. High-performance accelerometers were installed to measure the microtremors on the lining surface in each span. The specification parameters of the accelerometers are shown in Table 1. Three components of the microtremor in the vertical, horizontal and axial directions of tunnel were measured, respectively. The measurements lasted for 300 seconds for each sample with an interval of 0.001 second. The interfering signals which may be induced by the heavy traffic or measurement system are cut out. Accordingly a data record must be sufficiently long in order to reduce the influence of interfering signals. A typical example of the measured acceleration waves is shown in Fig. 4.

Table 1. Specification parameters of the accelerometer.

Fig. 2 Measurement system in in-situ tests. (a) Data acquisition unit. (b) Accelerometer.

Fig. 3 Accelerometer configurations in in-situ tests.

Fig. 4 An example of the acceleration waves.

The ‘spectrum peak-picking method’, which was widely used in spectrum analyses, was adopted for the peak frequency identification in data analyses. The Power Spectrum Density (PSD) *P(f)*, is given by

$$P(f)=\frac{1}{T}\left|X\left(f\right)\right|^2 \tag{1}$$

where *f* is the frequency, *T* is the time and *X(f)* is the frequency spectrum. The PSD of measured microtremor was calculated to acquire the peak frequency, by using the Welch’s averaged periodogram method implanted in MATLAB (MATLAB, 2003). In the Welch’s method, the PSD $P_{Welch}(f)$ can be calculated as (Welch, 1967):

$$P_{Welch}(f)=\frac{1}{F_s LU}\int_{-F_s/2}^{F_s/2}\left|W(f-f')\right|^2 P(f')df' \tag{2}$$

where *P(f)* is the PSD estimated by the discrete-time Fourier transform, F_s is the sampling frequency, *L* is the length of the data segments, *U* is the same normalization constant present in the definition of the modified periodogram and *W(f)* is the Fourier transform of the window function.

A hamming window with a length of 2048 and 50% data overlapping was adopted to smooth the curve and to reduce the leakage error. The spectrum resolution is 0.488 Hz. The PSD amplitudes were normalized by using the sum of the squares of the PSD corresponding to each frequency, as given by

$$NPSD(f)=P_{Welch}(f)\Big/\sqrt{\sum_{k=1}^{m}P_{Welch}(f)^2} \tag{3}$$

where *NPSD(f)* is the normalized PSD corresponding to the frequency *f* and *k* is the

number of frequency points. The average of all normalized PSD at an individual monitoring point was calculated and a so-called ANPSD spectrum was obtained:

$$ANPSD(f_k) = \frac{1}{n}\sum_{i=1}^{n} NPSD_i(f_k) \quad (4)$$

where $NPSD_i(f_k)$ is the normalized PSD for the frequency f_k at the monitoring point i. Using the averaged algorithm, those energy peaks were eliminated in each individual spectrum that were caused by short-term disturbances (e.g. the passing trucks during measurement). Meanwhile, the loss of peak frequencies on nodes where mode shape was zero could also be avoided.

The ANPSD spectrum of the measured signals was calculated, as shown in Fig.5. In the case of the healthy span S1 (Fig. 5a), three frequency peaks (56.6 Hz, 78.1 Hz and 86.9 Hz) can be found. In the case of span S2 (Fig.5b), in which voids exist, the ANPSD are distributed at a wide range of frequencies (30-100 Hz), where six frequency peaks (32.2 Hz, 68.4 Hz, 74.2 Hz, 78.1 Hz, 83.1 Hz and 88.9 Hz) can be identified. Its first peak frequency (32.2 Hz) is much smaller than that of span S1.

Fig.5 The normalized power spectrum in Satomi tunnel. (a) The healthy span S1. (b) The damaged span S2.

3. Numerical simulation of the microtremor of tunnel lining

Comparing with theoretical and experimental studies, the numerical simulation provides a convenient and low-cost approach to study the dynamic problems, especially when theoretical solutions are difficult to obtain. In this study, the tunnel

was simplified as a plane strain model and the numerical simulations were performed by using the DEM code of UDEC to investigate the microtremor vibration behavior of tunnel lining.

3.1 Numerical model for simulations

In these old tunnels that were built with the fore-poling method, the poling board was used instead of shotcrete so that incomplete contacts usually exist between rock mass and poling board, as shown in Fig. 6. The coring survey of lining showed that the temporary support (wooden boards) were closely bonded with the lining concrete. They were substantially consolidated subjected to the compression stresses from the surrounding rock mass and achieved high strength. Therefore, instead of treating the temporary support as a separate layer, we considered them as a part of concrete lining in numerical simulations for simplification. Their contacts with the surrounding rock mass were simplified to weak concrete-rock interfaces with low normal and shear stiffness. (i.e., the interfaces are treated as inner boundaries in the DEM) (UDEC 2000). The Mohr-Coulomb model and Coulomb slip model were adopted to represent the mechanical behavior of rock mass and interface, respectively. Those types of elements can effectively simulate the dynamic deformational behavior of rock mass, lining concrete and rock-concrete interface. The size of the numerical model and the positions of monitoring points (C1 and C2) are in accordance with the tested tunnel, as shown in Fig. 7. In the two-dimensional model, only the vibration histories in vertical and horizontal directions were recorded. Stress equivalent to an overburden of 35 m was applied on the upper boundary of the model. The physico-mechanical

properties of the surrounding rock mass and lining concrete are listed in Table 2, which are typical values of properties of the rock mass and concrete lining encountered in the construction of this tunnel. Since the microtremor doesn't cause the failure of rock mass and lining concrete, the tensile strength, cohesion and friction angle have no influence on the microtremor vibration behavior of the model.

A static equilibrium calculation was achieved before the start of dynamic analyses. In dynamical calculations, a stationary Gaussian white noise with power of 60 dBW and a frequency range of 0 to 100 Hz was input on the floor of tunnel in terms of a normal stress to represent the exciting source (e.g., passing vehicles). The Rayleigh damping with a ratio of 1% was utilized during dynamic calculations to represent the attenuation of materials. The boundaries of model were set as viscous boundaries to absorb the stress waves passing by and minimize wave reflections at boundaries. 32768 discrete time signal data at each monitoring point were recorded during numerical simulations with a sampling interval of 0.001s.

Fig.6 A cross-sectional view of the tunnel lining built by the fore-poling method.

Fig. 7 Model of numerical simulation.

Table 2. Material properties of rock mass and lining concrete used in the numerical simulations. The material properties of rock mass and lining concrete were acquired from in-situ investigation data of this tunnel.

3.2 Parameter optimization

The proper size of the spatial elements needs to be determined by taking into account the lowest velocity and the highest frequency of the wave propagation (Saenger et al. 2000). Rayleigh wave is generally considered as the lowest wave velocity (Zerwer et al., 2002) and its velocity V_R can be calculated by the following equation (Jaeger et al., 2007):

$$V_R = \frac{(0.874032 + 0.200396\nu - 0.0756704\nu^2)}{\sqrt{\frac{2(1-\nu)}{1-2\nu}}} V_P \tag{5}$$

where V_p is the longitudinal wave and ν is the Poisson's ratio of the concrete. In the numerical simulations, V_p of concrete was assumed as 3127 m/s, and V_R was calculated by Eq.(5) as 1857 m/s. Maximum frequency f_{max} of the white noise is 100 Hz, and the minimum wave length λ_{min} ($\lambda_{min} = V_R / f_{max}$) was calculated as 18.57 m. The element size should be smaller than approximately one-tenth of the wavelength associated with the highest frequency to simulate the wave transmission accurately (Kuhlmeyer and Lysmer, 1973). Hence, an element size of 0.2 m was adopted in this study in order to acquire the accurate results.

The supporting system has a great influence on the natural frequency of a structure, and the decrease of the contact stiffness of concrete-rock interface will reduce the natural frequency of the system (Chowdhury, 1990). It is difficult to directly measure the exact stiffness of concrete-rock interface through conventional mechanical testing; nevertheless, its stiffness can be estimated from the vibration properties of tunnel lining. The frequency responses of lining in low frequency range are defined by the

dynamic stiffness of the structural element which can be expressed by rock mass and concrete stiffness, concrete thickness and element support condition (Allen et al., 2005). After measuring the stiffness of rock mass and concrete and the thickness of concrete, the stiffness of concrete-rock interface, which plays the role of supporting, can be estimated based on the frequency response of the preliminary numerical studies.

A group of rock-concrete interfaces with different stiffness were simulated and their mechanical properties are listed in Table 3. The power spectra of obtained vibration histories in cases J-2-10, J-4-10 and J-2-100 were calculated to find the peak frequencies, as shown in Fig. 8a. The power spectra are influenced greatly by the normal stiffness (cases J-2-10 and J-4-10) while there is almost no variation at different shear stiffness (cases J-2-10 and J-2-100), which indicates that the normal stiffness rather than the shear stiffness plays dominated role in the frequency response of tunnel lining. With the decrease of the normal stiffness of interfaces, the peak frequency decreases, and the frequency difference between the first and the second modes increases, as shown in Fig. 8b. The peak frequency-normal stiffness curves approximate linear relations, indicating that the peak frequencies change proportionally with the normal stiffness of the rock-concrete interface. Based on the results of numerical simulations, the normal stiffness of the rock-concrete interface of the healthy span S1 can be estimated as around 265 MPa/m. By using this normal stiffness, the simulated peak frequencies for the first, second and third modes are 56.8 Hz, 77.2 Hz and 85.6 Hz (see Fig. 8b), respectively, which agree well with those

measured values (56.6 Hz, 78.1 Hz and 86.9 Hz), thus giving reasonable verification to the performance of the numerical approach used in this study.

The in-plane bending and symmetric mode shapes of the tunnel lining could be calculated based on the recorded vibration histories of lining. The mode shapes of models with different interface stiffness are similar, and one typical group of modes are plotted in Fig. 9.

Table 3. Material properties of rock-concrete interface used in the numerical simulations.

Fig. 8 Influence of the concrete-rock interface on the power spectrum. (a) The power spectra of tunnel lining corresponding to different normal and/or shear stiffness of concrete-rock interface in cases J-2-10, J-4-10 and J-2-100. (b) The relation between the peak frequency and the normal stiffness of concrete-rock interface in cases J-1-10, J-2-10, J-3-10, J-4-10 and J-5-10 (their mode shapes are plotted in Fig. 9.).

Fig. 9 One group of calculated mode shapes with the normal stiffness of 200 MPa/m (the ratio of shear to normal stiffness is 10%). (a) 48.0 Hz. (b) 71.8 Hz. (c) 81.0 Hz.

4. Numerical simulations of the model with voids

4.1 Influence of the voids

The voids can induce the increment of deformation and stress in the close vicinities,

causing serious damages on tunnel linings. For a planer model, the void location, the void depth and the void arc length are the main geometrical parameters of voids influencing the interacting between lining and rock mass. A series of simplified circular voids located at the arch and crown of tunnel lining where voids usually exist according to in-situ survey, were simulated to analyze the response of vibration behavior of lining to these parameters. A schematic view showing the parameters defining the status of voids is presented in Fig. 10, and the parameters of different cases are listed in Table 4. Mechanical properties of interface adopted the values of case J-2-10 in the following simulations. It should be noticed that the actual voids existing behind lining are three-dimensional in shape. To satisfy the plane strain assumptions in two-dimensional models, at here, voids with long length in the orientation of the tunnel axis were assumed.

Fig. 10 Schematic view of a void at rock-concrete interface. Void location: angle θ (VL), void arc length: sector angle γ (VS) and void depth: h (VD).

Table 4 Values of void parameters for different cases. Void location: angle θ (VL), void arc length: sector angle γ (VS) and void depth h (VD).

4.1.1 Influence of void location (angle θ)

The influence of void location defined by angle θ was analyzed by using the cases VL-1, VL-2 and VL-3 with a void depth of 0.6 m and a sector angle of 60°. Their

power spectra are shown in Fig. 11, peak frequencies are listed in Table 4 and the corresponding mode shapes are shown in Fig. 12.

In case VL-1, three frequency peaks (32.4 Hz, 68.7 Hz and 78.5 Hz) can be identified, and their mode shapes are symmetric, which are similar to the mode shapes of models without voids (Fig. 9). In cases VL-2 and VL-3, five frequency peaks can be identified (28.7 Hz, 38.3 Hz, 45.0 Hz, 65.1 Hz and 78.5 Hz in case VL-2; 26.3 Hz, 44.1 Hz, 65.1 Hz, 75.6 Hz and 80.8 Hz in case VL-3), and their mode shapes are non-symmetric because the void is not located on the central axis (Fig. 13). Except the first peak frequency, the peak frequencies of VL-2 are smaller than that of VL-3 with similar mode shapes. Meanwhile, the first peak frequency decreases gradually in these three cases (32.4 Hz in case VL-1, 28.7 Hz in case VL-2 and 26.3 Hz in case VL-3) as angle θ increases. In summary, as angle θ increases, the first peak frequency decreases and a few additional peak occurs due to the existence of voids not located on the central axis, which are in accordance with the in-situ measurement results in span S2 in which voids exist.

Fig. 11 The power spectrum of tunnel lining corresponding to different void locations (angle θ).

Fig. 12 The mode shapes of tunnel lining incase VL-1. (a) 32.4 Hz. (b) 68.7 Hz. (c) 78.5 H.

Fig. 13 The mode shapes of tunnel lining incase VL-3. (a) 26.3 Hz. (b) 44.1 Hz. (c) 65.1 Hz. (d) 75.6 Hz. (e) 80.8 Hz.

4.1.2 Influence of void arc length (sector angle γ)

The influence of void arc length defined by sector angle γ was analyzed using the cases with different void locations, but equivalent void depth of 0.6 m located in tunnel crown (cases VS-L0-1 ~ VS-L0-6) and in arch (cases VS-L60-1 ~ VS-L60-6), respectively. The calculated power spectra are shown in Fig. 14 and the relations between the peak frequency and the sector angle are shown in Fig. 15.

In the cases witha void in crown (θ = 0°), three frequency peaks can be identified (Fig. 14a). In the cases with a void in arch (θ = 60°), four frequency peaks (cases VS-L60-1, VS-L60-2 and VS-L60-3) and five frequency peaks (cases VS-L60-4 and VS-L60-5) can be identified, even though the second peak (around 45 Hz) is not as obvious as others, as shown in Fig. 14b. These reveal that additional vibration modes can be evoked due to the increase of void size (arc length). In Fig. 15, as the void size increases, peak frequencies decrease. The first peak frequency of the case with a void in crown descents sharply when γ <30°, while no obvious changes occur in other two peak frequencies (Fig. 15a). The first peak frequencies in the cases with avoid in arch are much smaller than those with voids in crown with the same void size, and the difference becomes larger when the void size is small. This indicates that the smaller peak frequency could be evoked when voids exist in arch.

Fig. 14 The power spectrum of tunnel lining corresponding to different void sector angles. (a) θ=0°. (b) θ=60°.

Fig. 15 The relations between the peak frequency and the void sector angles. (a) θ=0°. (b) θ=60°.

4.1.3 Influence of void depth *h*

The influence of void depth was analyzed by using the cases with different void depths when a void is located in tunnel crown (cases VD-L0-1, VD-L0-2, VD-L0-3 and VD-L0-4) and arch(cases VD-L60-1, VD-L60-2, VD-L60-3 and VD-L60-4), respectively. The calculated power spectra are shown in Fig. 16.

The variations of peak frequencies in different models are relatively small (less than 4 Hz). That is to say the void depth is probably a negligible parameter influencing the frequency response of tunnel lining with voids. However, the existence of voids usually reduces the thickness of the lining, causing a considerable reduction of the lining resistance. Especially in some occasional cases, the thickness of lining could drop to below 20 cm as shown in Cases VD-L0-1 and VD-L60-1, in which the steep decrease of lining thickness resulted in significant increase of stress. Therefore, attention needs to be paid on the void thickness which could not be identified by the frequency response, and additional damage detecting methods (e.g., boring) are recommended if necessary.

Fig. 16 The power spectrum of tunnel lining corresponding to different void depths. (a) θ=0°. (b) θ=60°.

4.1.4 Influence of multiple voids

Not only a single void, but also multiple voids are often detected between the rock mass and the tunnel lining in a single span (as shown in damaged span S2), and it is difficult to detect the void distribution exactly due to the limitation of the detection method. One model with two simplified voids (case V-L0-L60, one void on the crown and the other on arch as listed in Table 4) was adopted as a typical example to analyze the influences of multiple voids. The calculated power spectra are shown in Fig. 17.

Eight frequency peaks (24.3 Hz, 32.0 Hz, 47.5 Hz, 62.9 Hz, 69.6 Hz, 72.9 Hz, 80.6 Hz, and 87.6 Hz) could be identified, revealing that additional vibration modes can be evoked due to the increase of the void number. Meanwhile, the first peak frequency of this case is less than those of the cases VS-L0-3 and VS-L60-3, which indicates that the first peak frequency of the lining with multiple voids is less than that of the lining with a single void.

Fig. 17 The power spectrum of tunnel lining corresponding to multiple voids.

4.2 Influence of lining concrete type

The mechanical properties of three typical types of concrete that are commonly used in tunnel lining constructions are listed in Table 5. The variation of elastic modulus

usually causes changes in the peak frequency of tunnel lining, as demonstrated in Fig. 18. As the elastic modulus decreases, the peak frequencies also decrease gradually, and larger variation occurs in the second and third frequency peaks, showing that the peak frequencies in higher modes are more sensitive to the change of elastic modulus of lining concrete.

Table 5. Properties of different types of concrete used in numerical simulations

Fig. 18 The power spectrum of the tunnel lining constructed with different types of concrete.

4.3 Influence of rock type

Besides the rock-concrete interface and concrete lining, the surrounding rock mass remains as another key factor affecting the dynamic properties of the tunnel system. The properties of typical types of rocks are listed in Table 6 and the power spectra of tunnel lining supporting different rock types are shown in Fig. 19. Except the case of the weathered rock, there is no obvious influence of rock type on the peak frequencies and the variation of the spectrum amplitudes among them is less than 10%. In the case of the weathered rock, a number of peaks with low peak frequencies appear, rendering it difficult to clearly identify the peak frequencies. These results indicate that variations of peak frequencies of the tunnel lining that induced by flaws in lining (e.g., voids) can be identified obviously when the surrounding rock mass is unweathered,

while special attentions need be paid in the peak picking if the rock mass is highly weathered.

Table 6 Properties of rocks used in numerical simulations.

Fig. 19 The power spectrum of tunnel lining with different types of rocks.

5. Evaluation of influences of the voids on thelining stress

When a void exists behind a tunnel lining, the stress state of the lining will change significantly around the void into the state that the lining undergoes compression on the outer surface and tension on the inner surface. At here, outer surface stands for the surface of lining closer to the rock mass. The stress variation around the unsupported surfaces of the void may cause large deformation. These surfaces also contribute to the deflection of waves, and change the peak frequencies of lining. Furthermore, the unsupported length of the void changes the stiffness of the total supporting system, thus strongly affecting their frequency responses.

In-situ measurement and numerical simulation results have revealed that the first peak frequency of the lining decreases due to the existence of voids and is closely related to the geometrical parameters of the voids. The relations of the first peak frequency and the lining stresses (e.g. maximum principal stress σ_1, minimum principal stress σ_3, difference stress σ_1-σ_3 and maximum bending moment M) are shown in Fig. 20. Those presented indicators were normalized by ρhr and the first

peak frequency f was normalized by f_I, where ρ is the unit weight of the ground material, h is the overburden depth, r is the tunnel radius and f_I is the first peak frequency of the models without voids (i.e. case J-2-10) (Meguid and Dang, 2009). Best-fit curves of the data points (σ_1, σ_1-σ_3 and M) exhibit high determination coefficients (0.91 in Figs. 20ab and 0.85 in Fig. 20c), which means that σ_1, σ_1-σ_3 and M could be well estimated based on the first peak frequency by the best-fit function. There is a larger dispersion of data around the curves in Fig.20c (σ_3), and the estimated coefficient of determination is around 0.66.

In Fig. 20, the distribution of stress indicators (σ_1, σ_3, σ_1-σ_3 and M) exhibits a two-stage character. In the range of $f / f_I > 0.75$, the indicators are relatively small and vary in a small range, indicating that the tunnel lining is in a stable state with low stresses. Cases In-Ro-1~5 and In-Co-1~3 fall within this range, revealing that the influences of rock type and concrete type on stresses are small. In the range of $f / f_I < 0.75$, as the normalized frequency decreases, the indicators increase significantly. The voids in arch usually induce larger stress and deformation than that in crown with the same size. As the location angle and sector angle increase, the stress indicators increase and the first peak frequency decreases.

In cases VD-L0-2~4 and VD-L60-2~4 in which the void depth is no less than 0.4 m, the changes of stress indicators and the first peak frequency are located within a limited range. Therefore, the void depth could be considered as a secondary influencing parameter in most cases. However, in the cases VD-L0-1 and VD-L60-1, the significant increase in stress can be induced due to the steep decrease of lining

thickness, as marked by red circles in Figs. 20abd.

These limited numerical case studies suggest the large first peak frequency descending can be considered to be intimately linked with the stress indicators. In order to get more accurate results, a preliminary investment is necessary to acquire the tunnel information such as lining concrete type. The void location and size can be considered as the key parameters changing stress state of the tunnel lining in most cases. More in-situ measurements are necessary to enhance the reliability and applicability of this method.

Fig. 20 Evaluated results of lining safety state based on the first peak frequency (ρ is the unit weight of the ground material, h is the overburden depth and r is the tunnel radius). (a) The maximum principal stress (determination coefficient = 0.91). (b) The difference between the maximum and minimum principal stress (determination coefficient = 0.91). (c) The maximum bending moment (determination coefficient = 0.85). (d) The minimum principal stress (determination coefficient = 0.66).

6. Conclusions

This study presented a simple technique for the void identification of tunnel lining, through both in-situ measurements and numerical simulations of the microtremor characteristics of an aged mountain tunnel. By using the average of normalized power spectrum density (ANPSD) of microtremor, the peak frequencies of concrete lining in this tunnel were identified and the stress state of tunnel lining was evaluated based on the variation of first peak frequency. The influences of the geometrical parameters of

voids (location, size and depth), rock type and concrete type on the peak frequencies were also numerically investigated and were compared with in-situ measurements. The following conclusions are drawn from this study.

(1) In both in-situ measurements and numerical simulations, similar frequency response can be identified for the healthy span. The voids between the tunnel lining and the rock mass induced the decrease of the first peak frequency, and the additional frequency peaks occurred when the void was not located on the central axis. The decrease of the first peak frequency was found to be dependent mainly on the void size and location. The larger the void size and location angle, the largerthe decrease of the first peak frequency.

(2) The discontinuous contact between rockmass and lining concrete can be simplified as weak interfaces with low stiffness, which can be considered as an elastic supporting system during the dynamic calculation, and the normal stiffness of this weak interface can be estimated from the measured peak frequency.

(3) As the concrete stiffness decreases, the peak frequencies also decrease gradually and the peak frequencies in higher mode are more sensitive to the changes of lining stiffness. In the case of unweathered rock, the elastic modulus of rock has no obvious influence on the peak frequencies, while in the case of weathered rock, the peak frequency decreases slightly with the decrease of elastic modulus, and the identification of the peak frequencies become difficult due to the appearance of several small frequency peaks.

(4) The first peak frequency variation can be considered to be intimately linked with

the stress state. Except for the cases with extremely small void depth, the void location and size are key parameters changing the stress state of the tunnel lining.

The microtremor analysis method presented in this study only needs to measure the acceleration waves on the surface of tunnel lining, which is convenient for application, low in cost, and bringing negligible damage to the lining concrete. During the in-situ microtremor measurements, three points (one on crown, and other two on the arch of each side) are recommended in order to obtain the frequency information of the whole span. The peak frequency can be identified easily from the measured microtremor. A further study concerning the influence of crack generation and propagation induced by voids on frequency response is necessary. More in-situ measurements are needed to extend this method for future engineering practices and to give more comprehensive assessment of the microtremor dynamic properties of tunnel linings.

ACKNOWLEDGMENT: We wish to appreciate the Tokyo Sokki Co. Ltd and Geo-Research Institute for their help during in-situ measurements. Development of this study is partially supported by the Civil Engineering Division, Nagasaki Prefectural Government.

References

Allen G.D., Malcolm K.L., Claus G.P., 2005. Rapid and economical evaluation of concrete tunnel linings with impulse response and impulse radar non-destructive methods. NDT & E Int'l. 38, 181-186.

Chatelain J.-L., Guéguen P., Guillier B., Fréchet J., Bondoux F., Sarrault J., Sulpice P., Neuville J.-M., 2000. A user-friendly instrument dedicated to ambient noise (Microtremor) recording for site and building response studies. Seismol. Res. Lett. 71, 698-703.

Daniels D.J., 2004. Ground Penetrating Radar. 2nd ed. IEE Radar, Sonar, Navigation and Avionics Series, Institute of Electrical Engineers, London.

Gao Y., Jiang Y., Li B., Yamauchi, Y., 2012. Study on microtremor spectrum properties of tunnel lining. Proc. Symp. on Renew. Energ. Res. Appl. Nagasaki, 1-6.

Jiles D.C., 1990. Review of magnetic methods for nondestructive evaluation. NDT & E Int'l. 23(2), 83-92.

Ikeda Y., Suzuki Y., Suzuki Y., Adachi N., Nozawa T., 2010. Damage detection of actual building structures through singular value decomposition of power spectrum density matrices of microtremor responses. AIJ J. Technol. Des. 16(32), 69-74.

Jaeger J.C., Cook N.G.W., Zimmerman R.W., 2007. Fundamentals of Rock Mechanics 4th ed. Blackwell, Oxford.

Jiang Y., Li B., and Yamashita Y., 2009. Simulation of cracking near a larger underground cavern in a discontinuous rock mass using the expand distinct element method. Int. J. Rock Mech. Min. Sci. 46(1), 97-106.

Jiang Y., Gao Y., Li B., Ogawa Y., Yang L., 2012. Research on health assessment technique of tunnel lining based on power spectrum density characteristics of microtremors. J. JSCE Div. F1 68, I_111-I_118.

Júlio E.N.B.S., Rebelo C.A.D.S., Dias-da-Costa, D., 2008. Structural assessment of

the tower of the tower of the University of Coimbra by modal identification. Eng. Struc. 30(12), 3468-3477.

MATLAB Reference Guide, The Math Works, Inc., Natic, MA, 2003.

Kuhlmeyer R.L., Lysmer J., 1973. Finite element method accuracy for wave propagation problems. J. Soil Mech. & Found. Div. ASCE, 99(5), 421-427.

Lee, J.S., 2001. Installation of real-time monitoring system for high-speed railroad tunnel. J. Korean Tunnel. Assoc. 3, 63-67.

Meguid M.A., Dang H.K., 2009. The effect of erosion voids on existing tunnel linings. Tunn. Undergr. Sp. Tech. 24(3), 278-286.

Magalhas F., Cunha á., Cartano E., 2009. Online automatic identification of the modal parameters of a long span arch bridge. Mech. Syst. Signal Pr. 23(2), 316-329.

Michel C., Guéguen P., Bard P.Y., 2008. Dynamic parameters of structures extracted from ambient vibration measurements: an aid for the seismic vulnerability assessment of existing buildings in moderate seismic hazard regions. Soil Dyn. and Earthq. Eng. 28(8), 593-604.

Park S., Choi S., 2008. Development of methodology for estimating the effective properties of containment buildings. Korea Institute of Nuclear Safety, KINS/HR-836.

Peeters B., Maeck J. Roeck G.D., 2001. Vibration-based damage detection in civil engineering: excitation sources and temperature effects. Smart Mater. Struct. 10(3), 518-527.

Pierro E., Mucchi E., Soria L., Vecchio A., 2008. On the vibro-acoustical operational modal analysis of a helicopter cabin. Mech. Syst. and Signal Pr. 23, 1205-1217.

Poranski C.F, Greenawald E.C., Ham Y.S., 1996. X-ray backscatter tomography: NDT potential and limitations. Mater. Sci. Forum. 210-213, 211-218.

Saenger E.H., Gold N., Shapiro S.A., 2000. Modeling the propagation of elastic waves using a modified finite-difference grid. Wave Motion 31(1), 77-92.

Song K.I., Cho G.C., 2010. Numerical study on the evaluation of tunnel shotcrete using the Impact-Echo method coupled with Fourier transform and short-time Fourier transform. Int. J. Rock Mech. Min. 47(8), 1274-288.

Tuladhar R., Yamazaki F., Warnitchai P., Saita J., 2004. Seismic microzonation of the Greater Bangkok area using microtremor observations. Earthquake Eng. Struc. Dyn. 33(2), 211-225.

UDEC - user's manual. Minneapolis, MN: Itasca Consulting Group Inc. 2000.

Vestroni F., Capecchi D., 2000. Damage detection in beam structures based on frequency measurements. J. Eng. Mech. 126(7), 761-768.

Welch, P.D., 1967. The Use of Fast Fourier Transform for the Estimation of Power Spectra: A Method Based on Time Averaging Over Short, Modified Periodograms. IEEE Trans. Audio Electroacoust, AU-15, 70-73.

Wiehle C.K., 1964. Review of Soil-Structure Interaction. Proc. Symp. on Soil-Struc. Intera. Tucson Ariz. University of Arizona, 239-245.

Zerwer A., Cascante G., Hutchinson J., 2002. Parameter estimation in finite element simulations of Rayleigh waves. J. Geotech. Geoenviron. Eng. 128(3), 250-261.

Zhang C., Pekau O.A. Jin F., Wang G., 1997. Application of distinct element method in dynamic analysis of high rock slopes and blocky structure. Soil Dyn. Earthq. Eng.

16(6), 385-394.

Zhao J., Zhao X.B., Hefny A.M., Cai, J.G., 2006. Normal transmission of S-wave across parallel fractures with Coulomb slip behavior. J. Eng. Mech. 132(6), 641-650.

Zhao X.B., Zhao J., Cai J.G., Hefny A.M., 2008. UDEC modeling on wave propagation across fractured rock mass. Comput. Geotech. 35(1), 97-104.

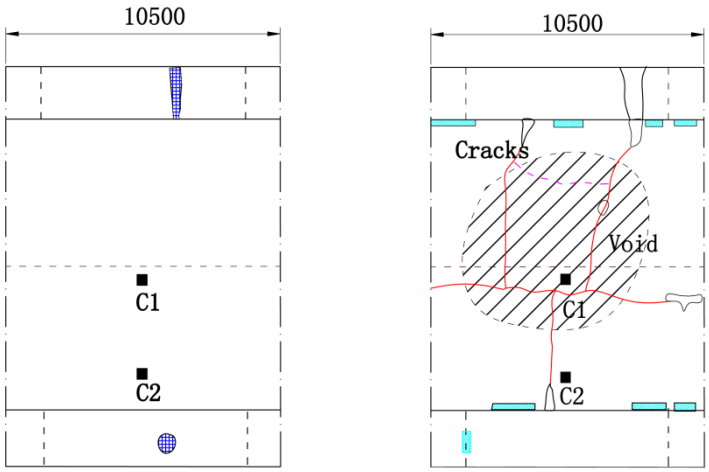

(a) (b)

Fig.1 Inspection results of spans S1 & S2. (a) S1:healthy span; (b) S2:damaged span, where voids, three transverse cracks and one axial crack exist.

(a) (b)

Fig. 2 Measurement system in field tests. (a) Data acquisition. (b) Accelerometer.

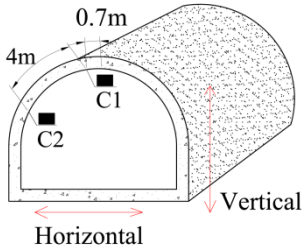

Fig. 3 Accelerometer configurations in field tests.

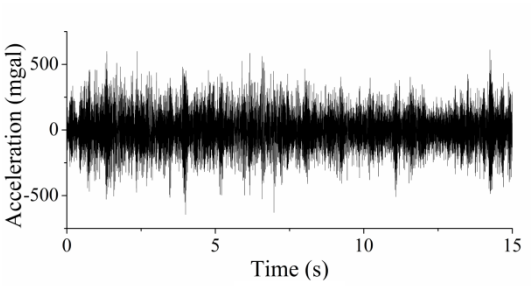

Fig.4 An example of the acceleration waves.

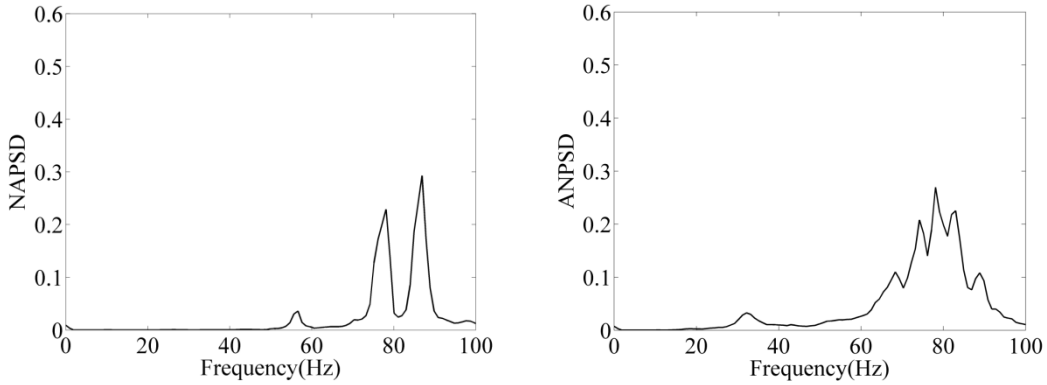

(a) (b)

Fig. 5 The normalized power spectrum in Satomi tunnel. (a) The healthy span S1. (b) The damaged span S2.

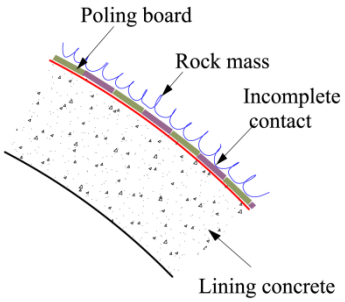

Fig. 6 A cross-sectional view of the tunnel lining built by the fore-poling method.

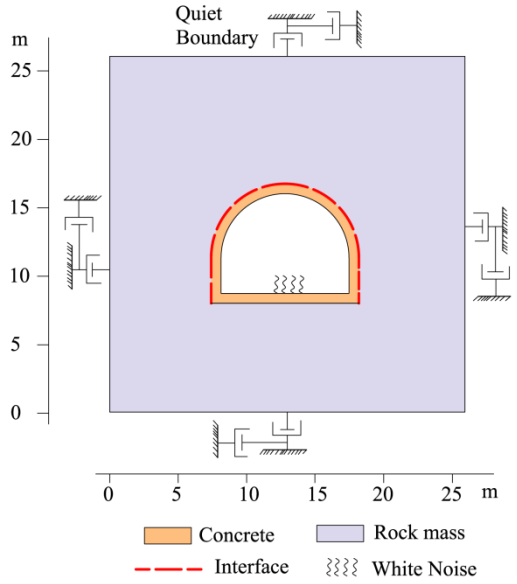

Fig. 7 Model of numerical simulation.

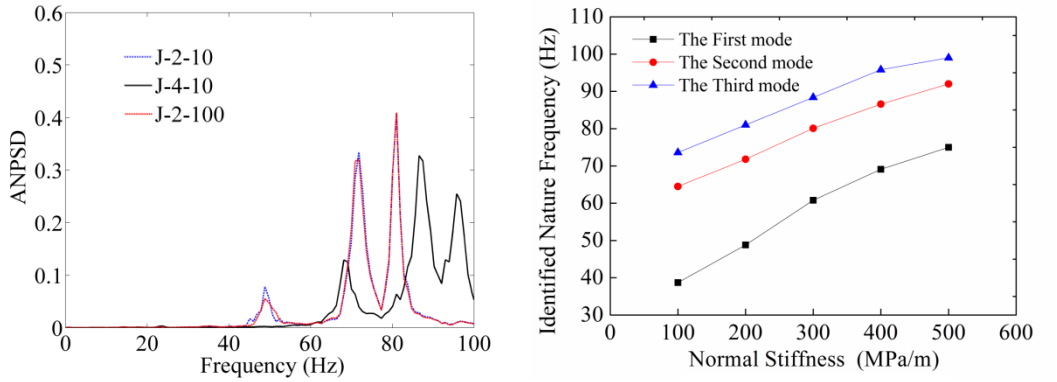

(a) (b)

Fig. 8 Influence of the concrete-rock interface on the power spectrum. (a) The power spectra of tunnel lining corresponding to different normal and/or shear stiffness of concrete-rock interface in cases J-2-10, J-4-10 and J-2-100. (b) The relation between the peak frequency and the normal stiffness of concrete-rock interface in cases J-1-10, J-2-10, J-3-10, J-4-10 and J-5-10 (their mode shapes are plotted in Fig. 9.).

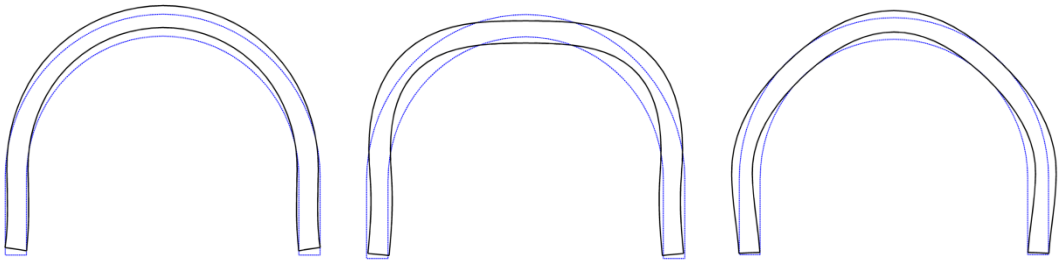

(a) (b) (c)

Fig. 9 One group of calculated mode shapes with the normal stiffness of 200MPa/m (the ratio of shear to normal stiffness is 10%). (a) 48.0 Hz. (b) 71.8 Hz. (c) 81.0 Hz.

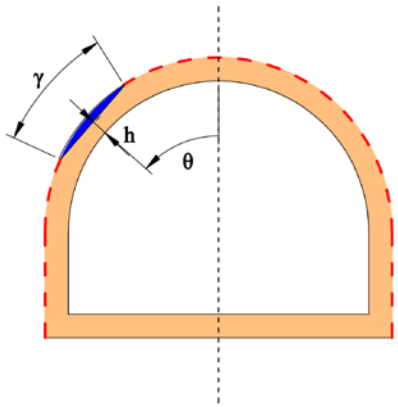

Fig. 10 Schematic view of a void at rock-concrete interface. Void location: angle θ (VL), void arc length: sector angle γ (VS) and void depth: h (VD).

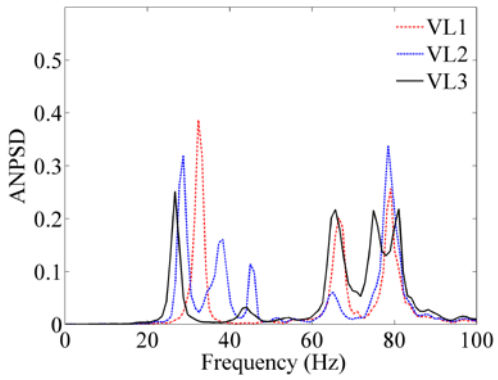

Fig. 11 The power spectrum of tunnel lining corresponding to different void locations (angle θ).

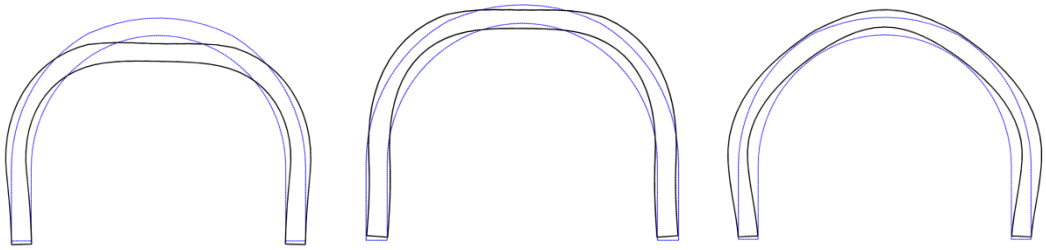

(a) (b) (c)

Fig. 12 The mode shapes of tunnel lining in case VL-1. (a) 32.4 Hz. (b) 68.7 Hz. (c) 78.5 Hz.

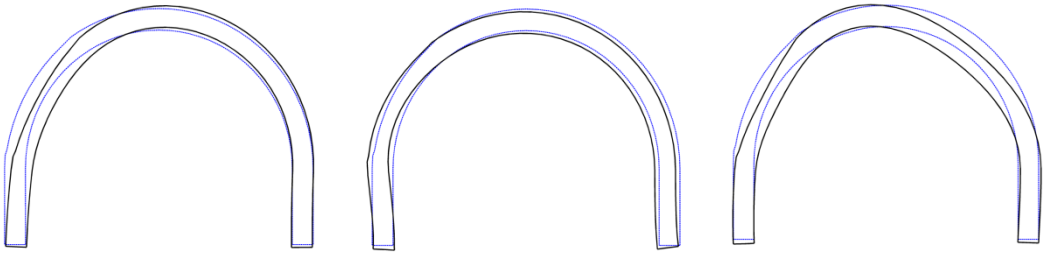

(a) (b) (c)

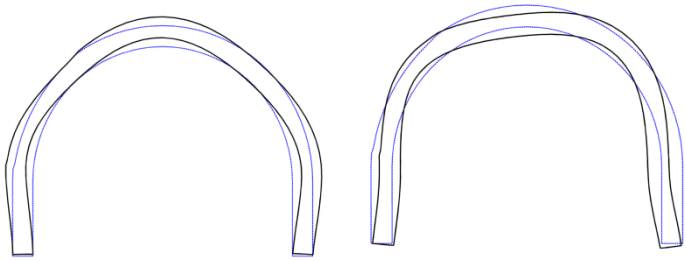

(d) (e)

Fig. 13 The mode shapes of tunnel lining in case VL-3. (a) 26.3 Hz. (b) 44.1 Hz. (c) 65.1 Hz. (d) 75.6 Hz. (e) 80.8 Hz.

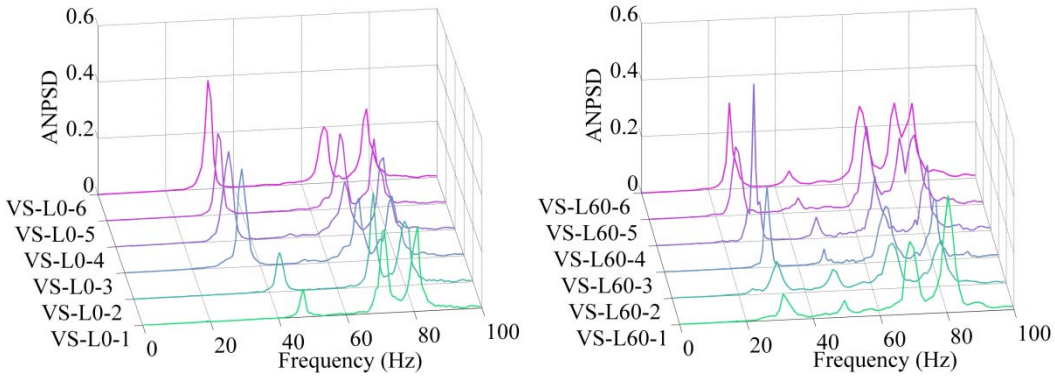

(a) (b)

Fig. 14 The power spectrum of tunnel lining corresponding to different void sector angles. (a) θ=0°; (b) θ=60°.

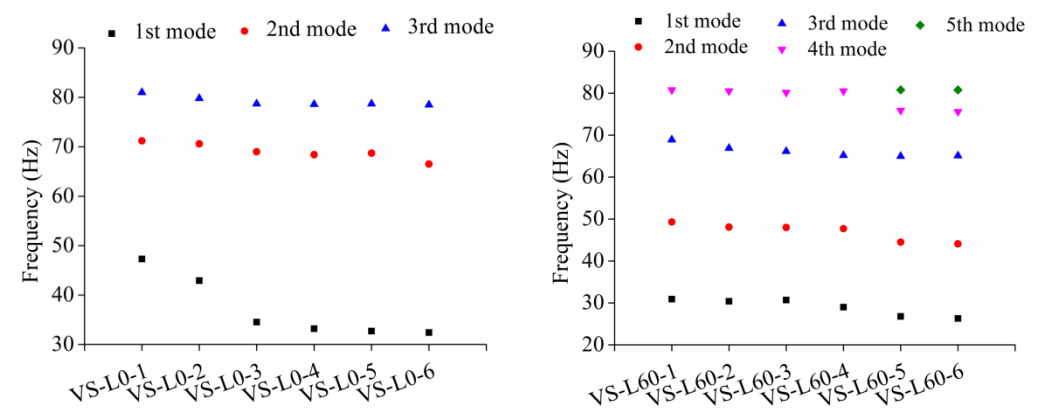

(a) (b)

Fig. 15 The relations between the peak frequency and the void sector angles. (a) θ=0°. (b) θ=60°.

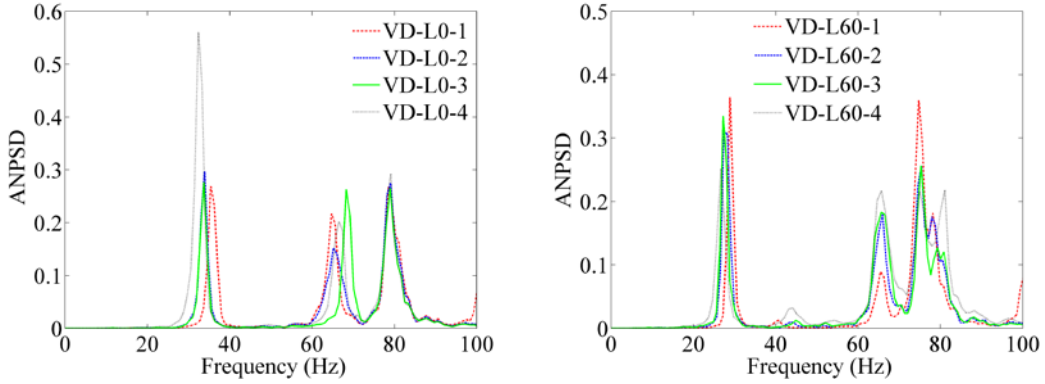

(a) (b)

Fig. 16 The power spectrum of tunnel lining corresponding to different void depths. (a) θ=0°. (b) θ=60°.

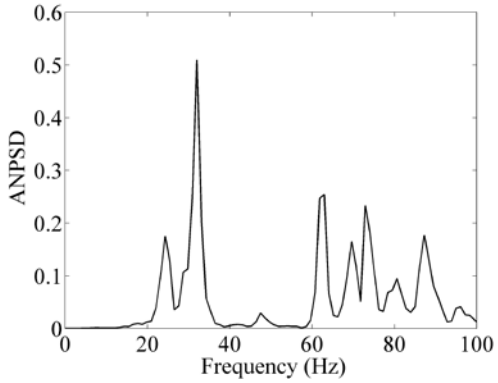

Fig. 17 The power spectrum of tunnel lining corresponding to multiple voids.

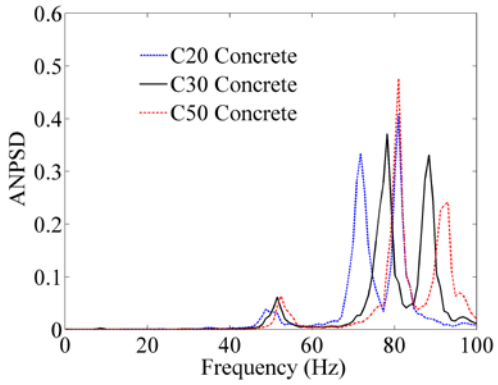

Fig. 18 The power spectrum of the tunnel lining with different types of concrete.

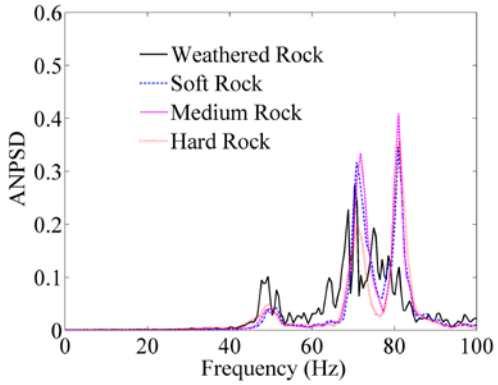

Fig. 19 The power spectrum of the tunnel lining with different types of rock masses.

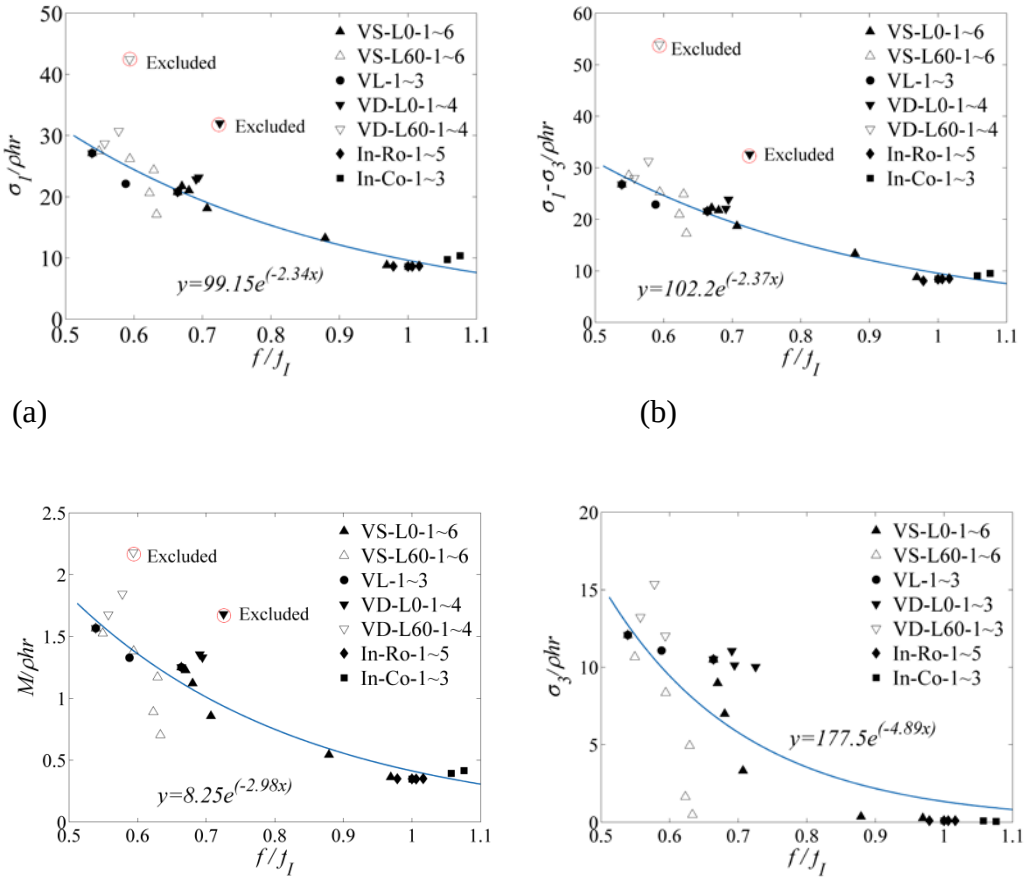

Fig.20 Evaluated results of lining safety state based on the first peak frequency (ρ is the unit weight of the ground material, h is the overburden depth and r is the tunnel radius). (a) The maximum principal stress (determination coefficient = 0.91). (b) The difference between the maximum and minimum principal stress (determination coefficient = 0.91). (c) The maximum bending moment (determination coefficient = 0.85). (d) The minimum principal stress (determination coefficient = 0.66).

Table 1. Specification parameters of the accelerometer.

Parameters	Units	Values
Type	-	LS-10C
Max. acceleration	m/s^2	±30
Frequency range	Hz	DC~100
Resolution	mgal	1
Size	mm	37(H)×37(W)×40(D)
Weight	g	220 (include Cord)

Table 2. Material properties of rock mass and lining concrete used in the numerical simulations. The material properties of rock mass and lining concrete were acquired from in-situ investigation data of this tunnel.

Parameters	Units	Rock mass	Concrete
Density	kg/m^3	2550	2500
Elastic modulus	GPa	30	22
Poisson ratio	-	0.22	0.28
Tensile strength	MPa	7.2	1.4
Cohesion	MPa	10.3	2.7
Friction angle	°	30	35

Table 3. Material properties of rock-concrete interface used in the numerical simulations.

Cases	Normal stiffness (MPa/m)	Shear stiffness (MPa/m)	Tensile strength MPa
J-5-10	500	50	0
J-4-10	400	40	0
J-3-10	300	30	0
J-2-100	200	2	0
J-2-10	200	20	0
J-1-10	100	10	0

Table 4 Values of void parameters for different cases. Void location: angle θ (VL), void arc length: sector angle γ (VS) and void depth: h (VD).

Case	θ (°)	γ (°)	h (m)	Peak frequencies(Hz)
VL-1	0	60	0.6	32.4, 66.5, 78.5
VL-2	30	60	0.6	28.7, 38.3, 45.0, 65.1, 78.5
VL-3	60	60	0.6	26.3, 44.1, 65.1, 75.6, 80.8
VS-L0-1	0	10	0.6	47.3, 71.2, 81.0
VS-L0-2	0	20	0.6	42.9, 70.6, 79.8
VS-L0-3	0	30	0.6	34.5, 69.0, 78.7
VS-L0-4	0	40	0.6	33.2, 68.4, 78.6
VS-L0-5	0	50	0.6	32.7, 68.7, 78.7
VS-L0-6	0	60	0.6	32.4, 66.5, 78.5
VS-L60-1	60	10	0.6	30.9, 49.3, 68.9, 80.8
VS-L60-2	60	20	0.6	30.4, 48.1, 66.9, 80.5
VS-L60-3	60	30	0.6	30.7, 48.0, 66.2, 80.2
VS-L60-4	60	40	0.6	29.0, 47.7, 65.2, 80.5
VS-L60-5	60	50	0.6	26.8, 44.5, 65.0, 75.9 80.8
VS-L60-6	60	60	0.6	26.3, 44.1, 65.1, 75.6 80.8
VD-L0-1	0	60	0.2	35.4, 64.3, 78.3
VD-L0-2	0	60	0.4	33.9, 65.7, 79.1
VD-L0-3	0	60	0.5	33.7, 68.3, 79.0
VD-L0-4	0	60	0.6	32.4, 66.5, 78.5
VD-L60-1	60	60	0.2	30.0, 40.2, 65.7,75.7, 80.4
VD-L60-2	60	60	0.4	28.2, 43.7, 65.7, 75.7, 78.8
VD-L60-3	60	60	0.5	27.2, 44.3, 65.5, 75.7, 80.4
VD-L60-4	60	60	0.6	26.3, 44.1, 65.1, 75.6, 80.8
V-L0-L60	0 & 60	30	0.6	24.3, 32.0, 47.5, 62.9, 69.6, 72.9, 80.6, 87.6

*Notation:*VL indicates the void location, VS indicates the void sector angle, VD indicates the void depth and L0 and L60 indicate the void location angle of 0° and 60° respectively.

Table 5. Properties of different types of concrete used in numerical simulations

Concrete type	Density (kg/m^3)	Elastic modulus (GPa)	Poisson's ratio
C20	2500	22	0.27
C30	2500	30	0.25
C50	2500	35	0.2

Table 6 Properties of rocks used in numerical simulations (Song and Cho 2010)

Material	Density (kg/m^3)	Elastic modulus (GPa)	Poisson ratio
Hard rock	2600	47	0.2
Medium rock	2550	30	0.22
Soft rock	2500	20	0.25
Weathered rock	2260	7	0.3